

对一个大单轴磁各向异性镍(II)配合物中的磁跃迁的直接观察

Chelsea N. Widener¹ Alexandria N. Bone¹ Mykhaylo Ozerov² Rachael Richardson³

路正光² Komalavalli Thirunavukkuarasu³ Dmitry Smirnov² 陈学太⁴ 薛子陵^{*,1}

(¹ 田纳西大学化学系, 诺克斯维尔市 37996, 美国)

(² 国家高磁场实验室, 佛罗里达州立大学, 塔拉哈西市 32310, 美国)

(³ 佛罗里达农工大学物理系, 塔拉哈西市 32307, 美国)

(⁴ 南京大学化学化工学院配位化学国家重点实验室, 南京 210023)

摘要: 最近 Ruamps 和同事发现三角双锥构型的 Ni(II)配合物[Ni(Me₆tren)Cl]ClO₄ (**1**, Me₆tren=tris(2-(dimethylamino)ethyl)amine)具有大的单轴磁各向异性(*J. Am. Chem. Soc.*, **2013**, **135**:3017-3026)。他们利用 HF-EPR 研究获得横向零场分裂(ZFS)参数 $E=1.56(5)$ cm⁻¹ 但未能确定轴向零场分裂参数 D 。在本工作中, 我们利用 0~17.5 T 和 5 K 的变磁场远红外光谱 (FIRMS) 来检测自旋基态 $S=1$ 中的 $M_S=\pm 1$ 和 $M_S=0$ 态之间的磁跃迁。在 FIRMS 中直接观察到 Zeeman 分裂态之间的跃迁, 得出轴向 ZFS 参数 $D=-110.7$ (3) cm⁻¹。我们对 **1** 的晶体结构进行了 Hirshfeld 表面分析, 揭示了 **1** 分子中的阳离子与阴离子之间以及分子之间的相互作用。

关键词: 镍配合物; 零场分裂磁跃迁; 单轴磁各向异性; 远红外光谱

中图分类号: O614.81+3

文献标识码: A

文章编号: 1001-4861(2020)06-1149-08

DOI: 10.11862/CJIC.2020.126

Direct Observation of Magnetic Transitions in a Nickel(II) Complex with Large Anisotropy

Chelsea N. Widener¹ Alexandria N. Bone¹ Mykhaylo Ozerov² Rachael Richardson³

LU Zheng-Guang² Komalavalli Thirunavukkuarasu³ Dmitry Smirnov² CHEN Xue-Tai⁴ XUE Zi-Ling^{*,1}

(¹Department of Chemistry, University of Tennessee, Knoxville, Tennessee 37996, United States)

(²National High Magnetic Field Laboratory, Florida State University, Tallahassee, Florida 32310, United States)

(³Department of Physics, Florida A&M University, Tallahassee, Florida 32307, United States)

(⁴State Key Laboratory of Coordination Chemistry, School of Chemistry and Chemical Engineering, Nanjing University, Nanjing 210023, China)

Abstract: Trigonal bipyramidal Ni(II) complex [Ni(Me₆tren)Cl](ClO₄) (**1**, Me₆tren=tris(2-(dimethylamino)ethyl)amine) has recently been shown by Ruamps and coworkers to possess large, uniaxial magnetic anisotropy (*J. Am. Chem. Soc.*, **2013**, **135**:3017-3026). Their HF-EPR studies gave rhombic zero-field-splitting (ZFS) parameter $E=1.56(5)$ cm⁻¹ for **1**. However, the axial ZFS parameter D has not been determined. We have used far-IR magnetic spectroscopy (FIRMS) at 0~17.5 T and 5 K to probe the magnetic transitions between the $M_S=\pm 1$ and $M_S=0$ states of the ground spin state $S=1$ in **1**. Direct observation of the transitions between Zeeman-split states in FIRMS gives axial ZFS parameter $D=-110.7$ (3) cm⁻¹. Hirshfeld surface analysis of the crystal structure of **1** has been performed, revealing the interactions between the cation and anion in a molecule of **1** as well as among the molecules of **1** in crystals.

Keywords: nickel complex; zero-field splitting transition; uniaxial magnetic anisotropy; far-IR magnetospectroscopy (FIRMS)

收稿日期: 2020-03-02。收修改稿日期: 2020-04-05。

Supported by U.S. National Science Foundation (No.CHE-1633870, CHE-1900296).

*通信联系人。E-mail: xue@utk.edu

0 Introduction

Magnetic properties of transition metal complexes have been actively studied recently, in part to understand the fundamental nature of the complexes and in part to probe their potential applications as single-molecule magnets (SMMs) and chemical qubits^[1-19]. For paramagnetic compounds with $S \geq 1$ and quenched orbital angular momenta, the ground electronic states of the compounds are split (zero-field splitting or ZFS) from second-order spin-orbital coupling involving the ground electronic states^[1-17]. The degree of the magnetic anisotropy is measured by axial (D) and rhombic (E) ZFS parameters^[15]. Ni(II) complexes displaying SMM properties have been reported^[20-25]. The d^8 complex in the current study, $[\text{Ni}(\text{Me}_6\text{tren})\text{Cl}](\text{ClO}_4)$ (**1**), contains a trigonal bipyramidal cation (Fig.1). In the trigonal crystal structure of **1** ($R3c$ space group, No.161), the $[\text{Ni}(\text{Me}_6\text{tren})\text{Cl}]^+$ cation sits on a 3-fold axis (Fig.1b). Thus, the crystallographic point group symmetry of the metal site (paramagnetic center) is axial and 3-fold. In other words, the (x, y) directions are degenerate. However, as discussed below, Jahn-Teller distortion leads to the breakup of the degeneracy.

The d orbitals in the Ni(II) ion in **1** are split by the ligand field into three sets as shown in Fig.1-Right. There are three electrons in the middle level, a degenerate set (e). Jahn-Teller distortion of the molecule of **1** to lower the energy leads to the splitting of the degenerate orbitals, as shown in Fig.1-Right.

With such five non-degenerate d orbitals in the Jahn-Teller distorted cation $[\text{Ni}(\text{Me}_6\text{tren})\text{Cl}]^+$, the orbital angular momentum is quenched. The two unpaired electrons in the Ni(II) complex ($S=1$) undergo second-order spin-orbital coupling with excited electronic states, leading to zero-field splitting (ZFS) of the triplet ground electronic state 3A_2 into the $M_S=0$ and doublet $M_S=\pm 1$ states. When the axial parameter $D < 0$, as in **1**, the molecule has an easy axis of magnetization in the z direction (or uniaxial magnetic anisotropy) which is typically assumed to be parallel to the C_3 axis. When $D > 0$, the molecule possesses an easy plane of magnetization in the x, y direction. In the Jahn-Teller distorted $[\text{Ni}(\text{Me}_6\text{tren})\text{Cl}]^+$, there is additional splitting of the degenerate $M_S=\pm 1$ states by the rhombic (E) parameter (Fig.2). The determination of the ZFS parameters is vital to understanding magnetic properties of the complex^[1-17].

Magnetometry (or direct-current magnetic measurement) is often employed to estimate the ZFS in metal complexes^[4], even though this is an indirect method based on essentially a multi-parameter fit of susceptibility and magnetization data by the spin-Hamiltonian. In addition, the sign of D is often not easily determined by magnetometry. High-frequency and high-field electron paramagnetic resonance (HF-EPR) has been used to study ZFS typically up to $\sim 33 \text{ cm}^{-1}$ (1 THz)^[4,26]. Ruamps and coworkers have used HF-EPR to probe a single crystal of $[\text{Ni}(\text{Me}_6\text{tren})\text{Cl}](\text{ClO}_4)$ (**1**) to give $E=1.56(5) \text{ cm}^{-1}$ and $g=2.34(7)$ ^[27]. The D value in **1** was estimated to be between -120 and

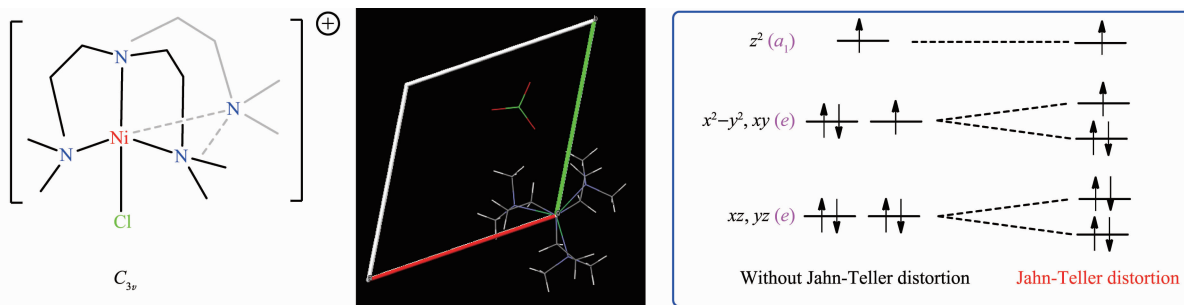


Fig.1 $[\text{Ni}(\text{Me}_6\text{tren})\text{Cl}]^+$ cation in **1** with local C_{3v} symmetry (Left); View of the cation and anion in **1** looking down the crystallographic c axis (Middle), showing that the cation is on a C_3 axis (a axis: red; b axis: green); Splitting of the d orbitals in the $[\text{Ni}(\text{Me}_6\text{tren})\text{Cl}]^+$ cation (Right), where the a_1 and e symbols refer to the symmetries of the d orbitals in the C_{3v} point group

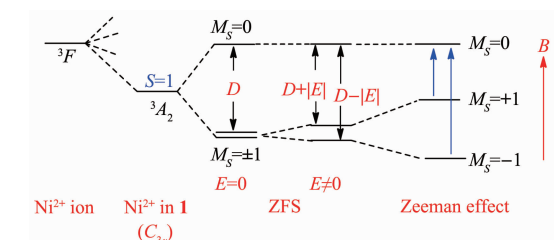


Fig.2 Ground-state triplet levels in high-spin, d^8 complexes with C_{3v} symmetry and uniaxial magnetic anisotropy ($D < 0$)

-180 cm^{-1} [27]. A subsequent semiempirical model study of the Ni(II) ion in **1** has been conducted to analyze the large ZFS [28].

FIRMS (far-IR magneto spectroscopy) is a direct technique to probe transitions such as those among ZFS states in transition metal complexes and magnetic transitions in f -element complexes [4,29-38]. It involves the use of magnetic fields in probing a sample by far-IR spectroscopy [31,37-40]. Earlier work by Brackett and Richards demonstrated that transitions among the ZFS states are magnetic-dipole allowed, making these transitions observable in far-IR [39-40]. In FIRMS, the sample is placed in variable magnetic fields. The Zeeman effect on the magnetic levels shifts the magnetic peaks in FIRMS, thus helping reveal and identify magnetic transitions in metal complexes that are too large to be measured by HF-EPR.

Understanding intermolecular interactions helps probe whether single-molecule magnets (SMMs) behave truly as individual molecules/magnets or the interactions among the molecules in the crystals of the compounds contribute to, *e.g.*, relaxation from magnetic excited states. Hirshfeld surface analysis is a newly developed method to study interactions of an individual molecule with its nearest neighbor molecules [41-44]. It is a simple approach of mapping void space in molecular crystals. A Hirshfeld surface is an isosurface calculated from the weight function $w(r)$ of the sum of spherical atom electron densities in Eq.(1):

$$w(r) = \frac{\rho_{\text{promolecule}}(r)}{\rho_{\text{promolecule}}(r)} = \sum_{A \in \text{molecule}} \rho_A(r) / \sum_{A \in \text{crystal}} \rho_A(r) \quad (1)$$

where $\rho_{\text{promolecule}}(r)$ =sum of the molecular electron density over the atoms in the molecule of interest (the promolecule); $\rho_{\text{procrystal}}(r)$ =similar sum over the crystal (the procrystal) [41-44].

The Hirshfeld surface leads to a visual 3D representation of the intermolecular close contacts in the crystal and computations of surface areas and volumes of the voids in the crystals [45]. Hirshfeld surface analysis is an excellent method to study molecular environment and interactions of compounds independent of the overall space group symmetry. We recently used the Hirshfeld surface analyses to study structures of metallocporphyrins Fe(TPP)Cl [46], M(TPP)(NO) (M=Fe, Co) [46], and Mn(TPP)X · solvent (X=Br, solvent=CHCl₃, CH₂Cl₂; X=I, solvent=CHCl₃, CDCl₃ and 1.5CHCl₃) [47]. These analyses show that intermolecular interactions contribute significantly to structural disorders of Fe(TPP)Cl and phase changes in M(TPP)(NO) (M=Fe, Co) [46].

In the current work, we have used FIRMS at 5 K to probe the ZFS transitions in **1**. By using $E=1.56 \text{ cm}^{-1}$ from the earlier HF-EPR studies [27], simulating the far-IR data gives $D=-110.7(3) \text{ cm}^{-1}$. Hirshfeld surface analyses of the crystal structure of **1** show the interactions among the ions (cations [Ni(Me₆tren)Cl]⁺ and anions ClO₄⁻) in the crystalline solid of **1**.

1 Experimental

Sample of [Ni(Me₆tren)Cl]ClO₄ (**1**) was prepared by the literature method [27].

1.1 Far-IR studies

Far-IR spectroscopic studies were conducted at the National High Magnetic Field Laboratory (NHMFL) at Florida State University. Transmittance far-IR spectra were collected using the powdered samples. The samples were mixed with eicosane and pressed into pellets that were approximately 1 mm thick. Spectra were collected at 4.5 K using a Bruker Vertex 80v FT-IR spectrometer coupled with a superconducting magnet (SCM 3) with fields up to 17 T.

1.2 Raman studies

Raman studies were conducted twice with two separate samples that were each prepared with an

unoriented single crystal of **1**. Data were collected by a backscattering Faraday geometry using a 532 nm laser at an 18 T superconducting magnet (SCM 2) or at a 14 T SCM in the electron magnetic resonance (EMR) in the dc field facility at NHMFL. Crystals of samples were cooled at 4.5 K. Collected scattered light was guided via an optical fiber to a spectrometer equipped with a liquid nitrogen-cooled CCD camera.

1.3 Hirshfeld surface calculations

Hirshfeld surfaces were calculated using Crystal Explorer (Version 17) software from the crystal-structure coordinates supplied in the format of crystallographic information file (CIF)^[48]. The reported X-ray CIF file of **1** at 100(1) K (CCDC: 893397)^[27] was used. Hirshfeld surfaces were calculated at an isovalue of $0.5 \text{ e} \cdot \text{au}^{-3}$. Void volumes were calculated using an isovalue of $0.002 \text{ e} \cdot \text{au}^{-3}$ ^[45].

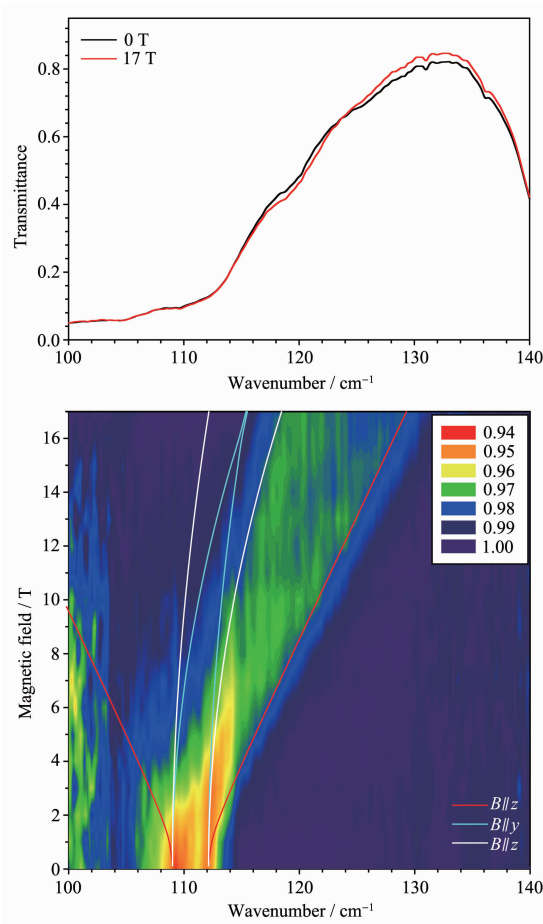
2 Results and discussion

2.1 FIRMS studies

The zero-field splitting (ZFS) in the Ni (II) compound was studied by the far-infrared magneto-spectroscopy (FIRMS) technique. This technique employs the Fourier-transform spectrometer to measure the magnetic response from the sample in the frequency domain (down to 20 cm^{-1}) while the magnetic field is fixed (in contrast to the electron paramagnetic resonance (EPR), where the frequency is fixed and magnetic field is swept). The sample was placed in a cryostat equipped by a vertical bore superconducting magnet and coupled to the spectrometer through the evacuated optical beam line. In this manner, the intensity of far-IR radiation transmitted through the sample was recorded with magnetic fields (up to 17 T) and at temperature of 4.5 K. In all measurements, the magnetic field was applied in Voigt geometry (magnetic field perpendicular to the wave vector of the radiation). All samples were a mixture of the eicosane matrix with microcrystalline powders and different trials were made for a variety of mixture ratios and sample thicknesses. The FIRMS spectra at 1 and 17 T near the magnetic peak and a contour plot of normalized

transmission are shown in Fig.3. Transmission of **1** normalized to the zero-field spectrum T_B/T_0 at 1~17 T is given in Fig.S1 in Supporting Information. FIRMS spectra of **1** at 1 and 17 T and a larger range of 20~720 cm^{-1} are given in Fig.S2. The range of 20~720 cm^{-1} is the entire far-IR range in the current work.

For the interpretation of far-IR data of **1**, the measured data are presented in terms of normalized transmission. The transmission spectrum measured at each magnetic field was normalized to the reference spectrum computed as an averaging of spectra for all magnetic fields and removing outlier points. Such normalization shows field-induced features masked at the original spectra due to the overlapping of the feature with phononic or intramolecular vibrational



Low-intensity regions indicate the presence of peaks; Solid lines are simulations by the EasySpin program for the Zeeman splittings in the $B//x$, $B//y$ and $B//z$ directions

Fig.3 (Top) Far-IR spectra of **1** at 0 and 17 T magnetic fields (100~140 cm^{-1}); (Bottom) Contour maps in 0~17 T magnetic fields

excitations. The quantitative contribution of magnetic excitations to absolute absorption of the sample is determined by the decrease in the normalized transmission. Therefore, this experimentally accessible quantity allows direct access to the transition intensity between field-dependent spin energy levels.

An in-house simulation program was written in Matlab for analysis of the magnetic field dependence of normalized transmission. The program is based on the EasySpin toolbox, allowing the calculations of the transition matrix element of the magnetic dipole transitions. Originally developed for the simulating and fitting a wide range of EPR spectra, the EasySpin toolbox provides frequency-domain simulation capabilities^[49]. The simulation is performed for single magnetic center with the $S=1$ spin Hamiltonian

$$\hat{H} = \mu_B \vec{B} \cdot \hat{g} \cdot \vec{S} + \vec{S} \cdot \hat{D} \cdot \vec{S} \quad (2)$$

where μ_B is Bohr magneton constant, \vec{B} is magnetic field vector, \vec{S} is vector spin operator, and $\hat{g} =$

$$\begin{pmatrix} g_x & 0 & 0 \\ 0 & g_y & 0 \\ 0 & 0 & g_z \end{pmatrix} \text{ is Landé tensors of the electron spin,}$$

$$\text{and } \hat{D} = \begin{pmatrix} -\frac{1}{3}D+E & 0 & 0 \\ 0 & -\frac{1}{3}D-E & 0 \\ 0 & 0 & -\frac{2}{3}D \end{pmatrix} \text{ is the ZFS}$$

tensor expressed by commonly used D and E zero-field splitting parameters. The input parameters $g_x=g_y=2.4$, $g_z=2.34$ and $E=1.56 \text{ cm}^{-1}$ were fixed and taken from the reference^[27]. D was only one variable parameter. The final absorption intensity spectra are obtained by introducing the line broadening parameter onto the calculated transition probabilities. The results of the simulation are shown in Fig.3-Bottom. The simulations yielded $D=-110.7(3) \text{ cm}^{-1}$.

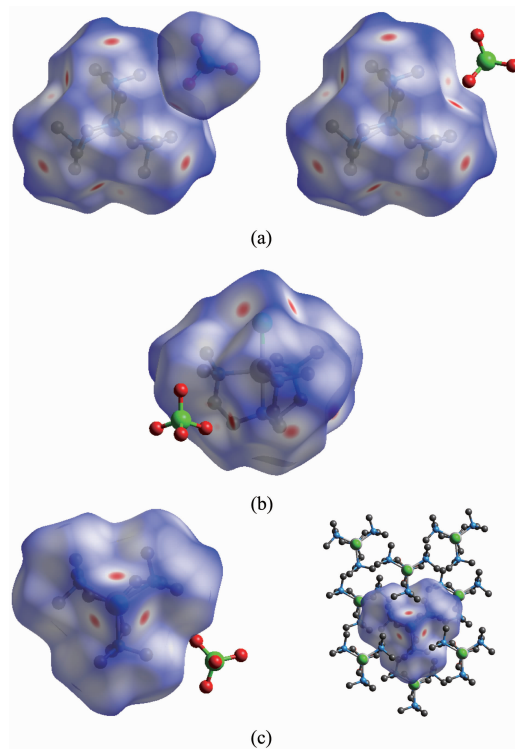
2.2 Raman spectra

Raman spectra of two separate cut crystals of **1** showed no magnetic feature (Fig.S3 ~S4). The ZFS transition in the range of the magnetic feature in far-IR spectra (Fig.3) was not observed in Raman spectra.

Although the ZFS transition was not observed in Raman spectra of $\text{Co}(\text{acac})_2(\text{H}_2\text{O})_2$ (acac^- =acetylacetonate), the spin-phonon coupling of the ZFS transition and nearby Raman-active phonons allow the ZFS transitions to obtain the intensities of the phonon transitions, leading to the observation of both ZFS and phonon peaks^[32]. However, there are apparently no Raman-active phonons that couple with the nearby ZFS transition in the Ni(II) complex **1** here (Fig.S3 ~S4). Fig.S4-Bottom shows spectra of 0 and 16 T Raman spectra at $50 \sim 594 \text{ cm}^{-1}$ which is the entire range in the current work.

2.3 Hirshfeld surface analyses

Hirshfeld surface of $[\text{Ni}(\text{Me}_6\text{tren})\text{Cl}]\text{ClO}_4$ (**1**) at 100(1) K is presented in Fig.4 with views from the top, bottom and side of the cation $[\text{Ni}(\text{Me}_6\text{tren})\text{Cl}]^+$. The red-white-blue coloring scheme in Fig.4 demonstrates decreasing contacts. Sites of close contacts are shown in red dots. Although there is



Semi-transparent view reveals the enclosed cation and anion

Fig.4 Hirshfeld surface of **1** showing normalized close distances of the pro-molecule at 100(1) K:

- (a) Top views looking down the N-Ni bond;
- (b) Side view; (c) Bottom views looking down the Cl-Ni bond with a packing diagram

close contact involving the “top” N atom on the C_3 axis, the void between two (2-(dimethylamino)ethyl) amine “arms” involves close contact with the anion ClO_4^- , as revealed in the top and side views in Fig. 4a~b. The bottom views (Fig. 4c) show that Cl^- ligand is in close contact with the H atoms of the methyl groups on the neighboring molecules. Additional views of the Hirshfeld surface with the packing diagram are given in Figs.S5 and S6 of Supporting Information.

The volumes and surface areas of the cation, anion ClO_4^- and the void in the crystal of **1** from the Hirshfeld surface analyses are given in Table 1.

Fingerprint plots, such as those in Fig.5 derived from the Hirshfeld surface^[50], provide a “fingerprint” of the intermolecular interactions in the crystal^[41-45]. They give a visual summary of the frequency of d_e and

d_i combinations across the surface of a molecule^[50]. d_e is the distance from the surface to the nearest nucleus external to the surface. d_i is the distance from the surface to the nearest nucleus internal to the surface^[43,51]. Each point on the 2D graph (Fig.5) represents a bin of width 0.001 nm in d_e and d_i with color indicating the fraction of surface points in that bin: blue (relatively few points), green (moderate fraction) and red (many points)^[43]. As Spackman and coworkers indicated, the d_e and d_i range varies

Table 1 Volumes and surface areas from Hirshfeld surface analyses

	Volume / nm^3	Surface area / nm^2
$[\text{Ni}(\text{Me}_6\text{tren})\text{Cl}]^+$ cation	0.383	2.95
ClO_4^- anion	0.071 8	0.906
Void	0.299	9.56

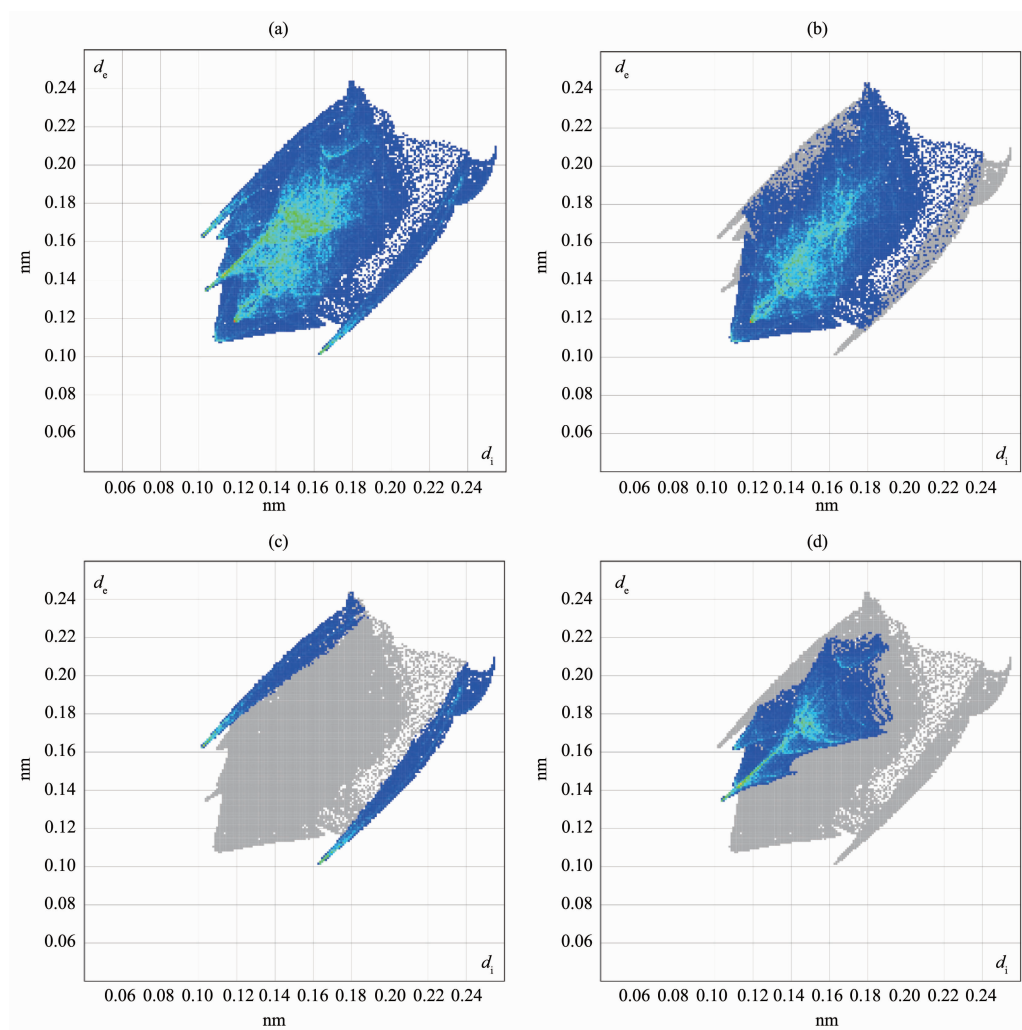


Fig.5 Fingerprint plots derived from the Hirshfeld surface of **1**: (a) All contacts; (b) H-H contacts (blue-green); (c) Cl-H contacts (blue-green); (d) O-H contacts (blue-green)

considerably across the Hirshfeld surface, and the change depends on the atoms in the molecule (*i.e.*, size dependence) and the type of intermolecular interaction involved (*i.e.*, interaction dependence)^[51]. Fig.5 shows that the closest contacts correspond to the minimum values of d_e+d_i are: 0.22 nm for H \cdots H (Fig. 5b); 0.26 nm for Cl \cdots H (Fig.5c); 0.24 nm for O \cdots H (Fig.5d). The H \cdots H contacts, as like \cdots like contacts are featured more along the diagonal (Fig.5b)^[50]. The ‘wings’ in Fig.5a are due to the Cl \cdots H (Fig.5c) and O \cdots H interactions (Fig.5d).

At present, the links between the results of the Hirshfeld surface analyses and relaxation of **1** from its magnetic excited (ZFS) state are not clear. However, it is believed that the interactions between the cation and anion in **1** and between molecules of **1** are part of the phonons (*i.e.*, both intramolecular and intermolecular vibrational modes) in the solid of **1**. Through spin-phonon coupling, the interactions revealed by the Hirshfeld surface analyses may contribute to the magnetic relaxation.

3 Conclusions

In summary, the current work led to explicit observation of the transitions between ZFS states in **1** by FIRMS, directly determining the axial ZFS parameter $D=-110.7(3)$ cm⁻¹. Thus, both ZFS parameters, D and the rhombic $E=1.56(5)$ cm⁻¹ from earlier HF-EPR work^[27], are obtained, providing an excellent example of using combined spectroscopies to determine accurately the spin Hamiltonian parameters in an SMM. Hirshfeld surface analyses of the crystal structure of **1** at 100(1) K give volumes and surface areas of the cation [Ni (Me₆tren)Cl]⁺, anion ClO₄⁻ and void in **1**. In addition, “fingerprints” of the intermolecular interactions reveal the intermolecular interactions in the crystal.

Acknowledgements: The authors thank financial support by the U.S. National Science Foundation (Grants No.CHE-1633870, CHE-1900296 to Z-L. X.) and the U.S. Department of Navy HBCU/MI program (K.T.). Part of this work was done at the National High Magnetic Field Laboratory, which is supported by U.S. National Science Foundation through

Cooperative Agreement DMR-1644779 and the State of Florida.

Supporting information is available at <http://www.wjhxsb.cn>

References:

- [1] Benelli C, Gatteschi D. *Introduction to Molecular Magnetism*. Weinheim: Wiley-VCH, **2015**:217-237
- [2] Frost J M, Harriman K L M, Murugesu M. *Chem. Sci.*, **2016**, **7**:2470-2491
- [3] Layfield R A. *Organometallics*, **2014**,**33**:1084-1099
- [4] Krzystek J, Telser J. *Dalton Trans.*, **2016**,**45**:16751-16763
- [5] McInnes E J L, Winpenny R E P. *Comprehensive Inorganic Chemistry: Vol.2*. Amsterdam: Elsevier, **2013**:371-395
- [6] Neese F, Pantazis D A. *Faraday Discuss.*, **2011**,**148**:229-238
- [7] Gao S. *Molecular Nanomagnets and Related Phenomena*. Heidelberg: Springer, **2015**:1-460
- [8] Zhang P, Zhang L, Tang J K. *Dalton Trans.*, **2015**,**44**:3923-3929
- [9] Liu J L, Chen Y C, Tong M L. *Chem. Soc. Rev.*, **2018**,**47**: 2431-2453
- [10] Craig G A, Murrie M. *Chem. Soc. Rev.*, **2015**,**44**:2135-2147
- [11] Rinehart J D, Long J R. *Chem. Sci.*, **2011**,**2**:2078-2085
- [12] Gatteschi D, Sessoli R. *Angew. Chem. Int. Ed.*, **2003**,**42**:268-297
- [13] Demir S, Jeon I-R, Long J R, et al. *Coord. Chem. Rev.*, **2015**, **289**:149-176
- [14] Dey M, Gogoi N. *Angew. Chem. Int. Ed.*, **2013**,**52**:12780-12782
- [15] Boča R. *Coord. Chem. Rev.*, **2004**,**248**:757-815
- [16] Shatruk M, Gómez-Coca S, Dunbar K R. *Molecular Magnetic Materials: Concepts and Applications*. Weinheim: Wiley-VCH, **2017**:29-77
- [17] Yamashita M, Katoh K. *Molecular Magnetic Materials: Concepts and Applications*. Weinheim: Wiley-VCH, **2017**: 79-101
- [18] Gatteschi D, Sessoli R, Villain J. *Molecular Nanomagnets*. Oxford: Oxford University Press, **2006**:1-317
- [19] Stavretis S E, Mamontov E, Moseley D H, et al. *Phys. Chem. Chem. Phys.*, **2018**,**20**:21119-21126
- [20] Marriott K E R, Bhaskaran L, Wilson C, et al. *Chem. Sci.*, **2015**,**6**:6823-6828
- [21] Miklovič J, Valigura D, Boča R, et al. *Dalton Trans.*, **2015**,**44**: 12484-12487
- [22] Lomjanský D, Moncol' J, Rajnak C, et al. *Chem. Commun.*, **2017**,**53**:6930-6932
- [23] Craig G A, Sarkar A, Woodall C H, et al. *Chem. Sci.*, **2018**, **9**:1551-1559

- [24]Titiš J, Rajnák C, Valigura D, et al. *Dalton Trans.*, **2018**,**47**: 7879-7882
- [25]Titiš J, Chrenková V, Rajnák C, et al. *Dalton Trans.*, **2019**, **48**:11647-11650
- [26]Chen L, Wang J, Wei J M, et al. *J. Am. Chem. Soc.*, **2014**, **136**:12213-12216
- [27]Ruamps R, Maurice R, Batchelor L, et al. *J. Am. Chem. Soc.*, **2013**,**135**:3017-3026
- [28]Rudowicz C, Açıkgöz M, Gnutek P. *J. Magn. Magn. Mater.*, **2017**,**434**:56-61
- [29]Ray K, Begum A, Weyhermuller T, et al. *J. Am. Chem. Soc.*, **2005**,**127**:4403-4415
- [30]Rechkemmer Y, Fischer J E, Marx R, et al. *J. Am. Chem. Soc.*, **2015**,**137**:13114-13120
- [31]Rechkemmer Y, Breitgoff F D, van der Meer M, et al. *Nat. Commun.*, **2016**,**7**:10467
- [32]Bunting P C, Atanasov M, Damgaard-Moller E, et al. *Science*, **2018**,**362**:eaat7319
- [33]Jiang S D, Maganas D, Levesanos N, et al. *J. Am. Chem. Soc.*, **2015**,**137**:12923-12928
- [34]Switlicka A, Machura B, Penkala M, et al. *Inorg. Chem.*, **2018**,**57**:12740-12755
- [35]Hay M A, Sarkar A, Craig G. *Chem. Sci.*, **2019**,**10**:6354-6361
- [36]Haas S. *Thesis for the Doctorate of University of Stuttgart*. **2015**.
- [37]Moseley D H, Stavretis S E, Thirunavukkuarasu K, et al. *Nat. Commun.*, **2018**,**9**:2572
- [38]Stavretis S E, Moseley D H, Fei F, et al. *Chem. Eur. J.*, **2019**,**25**:15846-15857
- [39]Brackett G C. *Thesis for the Doctorate of University of California Berkeley*. **1970**.
- [40]Brackett G C, Richards P L, Caughey W S. *J. Chem. Phys.*, **1971**,**54**:4383-4401
- [41]McKinnon J J, Jayatilaka D, Spackman M A. *Chem. Commun.*, **2007**,**37**:3814-3816
- [42]Spackman M A, Jayatilaka D. *CrystEngComm*, **2009**,**11**:19-32
- [43]Spackman M A, McKinnon J J. *CrystEngComm*, **2002**,**4**:378-392
- [44]McKinnon J J, Spackman M A, Mitchell A S. *Acta Crystallogr. Sect. B*, **2004**,**B60**:627-668
- [45]Turner M J, McKinnon J J, Jayatilaka D, et al. *CrystEngComm*, **2011**,**13**:1804-1813
- [46]Hunter S C, Smith B A, Hoffmann C M, et al. *Inorg. Chem.*, **2014**,**53**:11552-11562
- [47]Bone A N, Stavretis S E, Krzystek J, et al. *Polyhedron*, **2020**, doi:[https://doi.org/ 10.1016/j.poly.2020.114488](https://doi.org/10.1016/j.poly.2020.114488)
- [48]Turner M J, McKinnon J J, Wolff S K, et al. CrystalExplorer17. <https://crystalexplorer.scb.uwa.edu.au/downloads.html>
- [49]Stoll S, Schweiger A. *J. Magn. Reson.*, **2006**,**178**:42-55
- [50]Fingerprint plots; Website:http://crystalexplorer.scb.uwa.edu.au/wiki/index.php/Fingerprint_Plots
- [51]Hirshfeld surface properties; Website:http://crystalexplorer.scb.uwa.edu.au/wiki/index.php/Surface_Properties